

Propagation of thermal excitations in a cluster of vortices in superfluid $^3\text{He-B}$

J. J. Hosio,^{1,*} V. B. Eltsov,¹ R. de Graaf,¹ M. Krusius,¹ J. Mäkinen,¹ and D. Schmoranzner²

¹*Low Temperature Laboratory, P.O. Box 15100, FI-00076 AALTO, Finland*

²*Faculty of Mathematics and Physics, Charles University, Ke Karlovu 3, CZ-121 16 Prague, Czech Republic*

(Received 6 September 2011; revised manuscript received 16 November 2011; published 12 December 2011)

We describe the first measurement on Andreev scattering of thermal excitations from a vortex configuration with known density, spatial extent, and orientations in $^3\text{He-B}$ superfluid. The heat flow from a blackbody radiator in equilibrium rotation at constant angular velocity is measured with two quartz tuning fork oscillators. One oscillator creates a controllable density of excitations at $0.2T_c$ base temperature and the other records the thermal response. The results are compared to numerical calculations of ballistic propagation of thermal quasiparticles through a cluster of rectilinear vortices. We find good agreement which supports the current understanding of Andreev reflection.

DOI: [10.1103/PhysRevB.84.224501](https://doi.org/10.1103/PhysRevB.84.224501)

PACS number(s): 67.30.hb, 07.20.Mc, 74.45.+c

I. INTRODUCTION

Measurements of quantized vortices and attempts to develop methods for the visualization of different vortex configurations have been central in superfluid studies. Recent interest has focused on quantum turbulence.¹ In Bose-Einstein-condensed atom clouds, motion of vortices has been investigated with optical means.² In the long-studied case of superfluid ^4He , vortices can be detected, e.g., by ion trapping on vortex cores or second sound attenuation,³ while recent work on turbulence studies has been making use of transmission measurements of charged vortex rings⁴ or trapping of micron-sized tracer particles in vortex tangles,⁵ as well as analyzing the drag force exerted on vibrating structures.⁶ In superfluid ^3He , the traditional method to study vortices is nuclear magnetic resonance.⁷ The superfluid flow due to quantized vortices modifies the order parameter field and, thus, the NMR signal. In uniform rotation, a resolution of a single vortex can be obtained^{8,9} in a measurement of the counterflow velocity at temperatures $T > 0.5T_c$. At very low temperatures, in the limit $T/T_c \ll 1$, a powerful tool is the Andreev scattering of thermal excitations. This technique has been developed and exploited at the University of Lancaster.¹⁰

Hitherto the Andreev scattering technique has only been used to detect turbulent vortex tangles, which for interpretation have been assumed to be homogeneous and isotropic, but which in practice are of unknown density and poorly known spatial extent. Thus, it has not been possible to compare theoretical predictions of heat transport in vortex systems directly to experimental results. In this work, we provide such a comparison and justify the use of the Andreev reflection technique as a visualization method of vortices in superfluid $^3\text{He-B}$ in the limit of vanishing normal fluid density.

II. ANDREEV REFLECTION FROM VORTEX LINES

In the ballistic regime of quasiparticle transport, the mean-free path of thermal excitations is longer than the dimensions of the container. Therefore, thermal equilibrium is obtained via interaction of the quasiparticles and the container walls, and the collisions between excitations can be neglected. In the presence of vortices, the superfluid flow field around the vortex lines can constrain the quasiparticle trajectories.

In the rest frame of the superfluid condensate, the BCS dispersion relation $E(\mathbf{p})$ is symmetrical, and the minimum energy is the pressure-dependent superfluid energy gap Δ . The standard picture of Andreev reflection considers an excitation moving toward an increasing energy gap.¹¹ In $^3\text{He-B}$, the superfluid flow field modulates the minimum in the excitation spectrum. Using the notation of Barenghi *et al.*,¹² the energy E of the excitation with momentum \mathbf{p} in the flow field around a vortex is given by

$$E(\mathbf{p}) = \sqrt{\varepsilon_p^2 + \Delta^2} + \mathbf{p} \cdot \mathbf{v}_s, \quad (1)$$

where $\varepsilon_p = p^2/2m^* - \varepsilon_F$ is the effective kinetic energy of the excitation measured with respect to the Fermi energy ε_F and $p = |\mathbf{p}|$. Excitations with $\varepsilon_p > 0$ are called quasiparticles, and excitations with $\varepsilon_p < 0$ are called quasiholes. For quasiparticles the group velocity $\mathbf{v}_g(E) = dE/d\mathbf{p}$ is parallel to the momentum \mathbf{p} , whereas for quasiholes it is antiparallel. Our experiments are performed at the 29 bar pressure, at which the effective mass $m^* \approx 5.42m_3$, where m_3 is the mass of a ^3He atom. The superfluid velocity \mathbf{v}_s is proportional to the gradient of the phase φ of the order parameter, i.e., $\mathbf{v}_s = \hbar/(2m_3)\nabla\varphi$. If we consider a vortex oriented along the z axis in cylindrical coordinates (r, ϕ, z) , this becomes $\mathbf{v}_s = \kappa/(2\pi r)\hat{\phi}$, where $\kappa = h/2m_3 \approx 6.62 \times 10^{-8} \text{ m}^2/\text{s}$ is the circulation quantum, and $\hat{\phi}$ the azimuthal unit vector.

The consequence of the interaction term $\mathbf{p} \cdot \mathbf{v}_s$ is that an excitation traveling at constant energy may not find a forward-propagating state due to the superflow gradient $\nabla\mathbf{v}_s$ along the flight path. When the excitation reaches the minimum of the spectrum, its group velocity changes sign, and it retraces its trajectory as an excitation on the other side of the minimum. In other words, a quasiparticle Andreev reflects as a quasihole and vice versa with a very small momentum transfer.¹³

Let us consider a beam of excitations incident on a single straight vortex. On one side of the vortex, the flow parallel to the group velocity of the excitation reflects quasiparticles, and on the other side the antiparallel flow reflects quasiholes. An excitation is Andreev reflected if its energy satisfies $E \leq \Delta + p\kappa/(2\pi b)\sin\theta$. Here θ is the inclination angle of the excitation trajectory measured with respect to the vortex line and b the impact parameter. At temperature T the mean excitation energy is $\bar{E} = \Delta + k_B T$. In our experiments

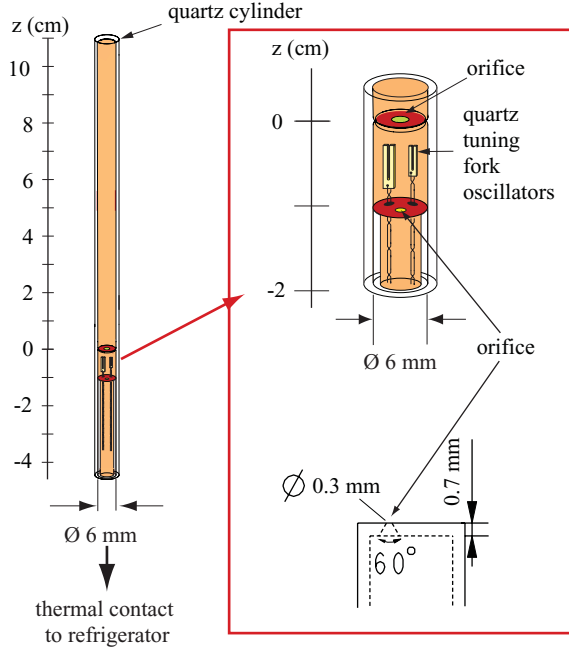


FIG. 1. (Color online) The experimental setup. The upper experimental volume modeled as a black body radiator is separated from the heat exchanger volume at the bottom by a division plate with a conical orifice with the minimum diameter of 0.3 mm. The upper division plate with a 0.75 mm diameter aperture is not relevant to the measurement described here. The BBR houses two quartz tuning fork oscillators, one acting as heater, and the other as thermometer.

$k_B T \sim 0.1\Delta$, and the momentum p is close to the Fermi momentum $p_F \approx 9.26 \times 10^{-25}$ kgm/s, so a typical excitation is reflected if $b < 5p_F \kappa \sin \theta / (\pi \Delta)$. For an excitation with $\theta \approx \pi/4$, this translates to $\sim 1 \mu\text{m}$, which is about two orders of magnitude larger than the coherence length $\xi \approx 15$ nm and the vortex core radius. Thus, in a typical experimental situation the probability of an excitation scattering off a vortex core is negligible compared to the cross section for Andreev scattering from the flow field around the vortex.

III. EXPERIMENTAL METHODS

In our experiment, we study the heat transport by excitations through a cluster of vortices. Bradley and coworkers did a similar measurement with a vortex tangle reflecting the excitations.¹⁴ Our experiment is made in a fused quartz cylinder filled with $^3\text{He-B}$ (see Fig. 1). The cylinder is divided into two parts by a 0.7-mm-thick quartz division plate with a 0.3-mm orifice. The lower part consists of a 30-mm-long, 3.6-mm-inner-diameter tube, which opens to a heat exchanger made out of sintered silver. The sinter provides good thermal contact with the nuclear cooling stage so that the superfluid ^3He below the orifice can be cooled down to below $0.14T_c$. The upper part can be modeled as a blackbody radiator (BBR), an enclosure with a weak thermal link to the outside superfluid ^3He via the small orifice in the division plate.¹⁵ Our BBR consists of a 12-cm-long section of the quartz tube with 6-mm inner diameter. This volume is furnished with two mechanical resonators, one acting as a thermometer and the other as a

heater. The heater is used for generating a beam of ballistic quasiparticles through the orifice.

Our resonators are commercial quartz tuning forks, which have recently been characterized for probing quantum fluids.^{16,17} The forks are made of piezoelectric quartz crystals with electrodes deposited on the surface. When driven with alternating voltage, the two prongs of the fork oscillate in antiphase producing a current I , which is proportional to the prong tip velocity v_p . The heater fork signal is amplified with a room-temperature I/V converter¹⁸ before being fed to a two-phase lock-in amplifier. This was found to be important to reduce capacitive losses in the signal line, and thus to measure accurately the signal amplitude which corresponds to the power generated by the fork. The thermometer fork has 32 kHz resonance frequency, a prong cross section of $0.10 \times 0.24 \text{ mm}^2$ and a length of 2.4 mm. The heater fork has a higher resonance frequency, 40 kHz, to prevent any interference between the forks. The prongs of the heater are 2.9 mm long and the cross section is $0.36 \times 0.44 \text{ mm}^2$.

In our temperature range, the resonance width of the tuning fork depends only on the damping from ballistic quasiparticles. The dependence of the linewidth Δf on temperature and prong velocity is given by

$$\Delta f = \Delta f_{\text{int}} + a e^{-\Delta/k_B T} \left(1 - \lambda \frac{p_F}{k_B T} v_p \right), \quad (2)$$

where λ is a geometrical factor close to unity.¹⁹ The second term in the parentheses is due to Andreev reflection of thermal quasiparticles from the potential flow field created by the fork prongs moving the liquid around them. In our experiments v_p is small, and the velocity-dependent term in Eq. (2) can be neglected. Thus, calibrating the fork to act as a thermometer requires determining only the geometry-dependent factor a . The thermometer is calibrated at $0.33T_c$ against a ^3He -melting curve thermometer, which is thermally coupled to the heat exchanger. Our calibration gives $a \approx 17500$ Hz for the detector. The intrinsic damping of the fork was measured to be $\Delta f_{\text{int}} \approx 14$ mHz at $T \sim 10$ mK in a vacuum, which translates to a quality factor $Q \sim 2 \times 10^6$.

The rough surface of the sinter with a grain size close to the vortex core diameter provides excellent spots for vortices to nucleate. Thus, the critical rotation velocity Ω_c for vortex formation is below 0.1 rad/s in the bottom section of the long quartz tube. In the equilibrium vortex state in uniform rotation, the bottom section becomes filled with rectilinear vortices oriented along the rotation axis. To create the vortex array, which Andreev reflects a part of the heat back to the BBR, we rotate our system at constant angular velocity Ω around the axis of the container tube. The vortex density in the equilibrium state is determined by minimization of the free energy in the rotating frame and is given by the solid-body-rotation value $n_v = 2\Omega/\kappa$. The array is isolated from the container wall by a narrow annular vortex-free layer. The width of the vortex-free region $\sqrt{\kappa/(\sqrt{3}\Omega)}$ is only slightly larger than the intervortex distance.²⁰

To make sure that we have the equilibrium number of vortices in the container, we first rapidly increase the rotation velocity to some value which is higher than the target velocity for the measurement. Then we go to the final velocity and wait

for the system to settle to the equilibrium vortex state after the annihilation of the extra vortices and the slow relaxation of the vortex array. In our experimental conditions the relaxation takes about 1 h.

All the power entering our experimental volume modeled as a blackbody radiator must leave through the hole at the bottom as a flux of energy-carrying excitations. Assuming thermal equilibrium inside the BBR the power is given by

$$\dot{Q}(\Omega) = \int N(E) v_g(E) E f(E) \mathcal{T} dE dx dy d\phi d\theta, \quad (3)$$

where $N(E)$ and $f(E)$ are the quasiparticle density of states and the Fermi distribution function, respectively. In the limit $k_B T \ll \Delta$ the latter reduces to the Boltzmann distribution $f(E) = e^{-E/k_B T}$. The transmission function $\mathcal{T} = \mathcal{T}(E, x, y, \phi, \theta, \Omega)$ is equal to 1 if an excitation leaving the BBR [at position (x, y) on top of the orifice to direction (ϕ, θ)] reaches the sinter and 0 if it is reflected back. The integration goes over the cross section of the orifice, $\phi \in (0, 2\pi)$, $\theta \in (0, \pi/2)$, and $E \in (\Delta, \infty)$. The power generated inside the radiator can now be expressed as the sum of the Ω -dependent residual heat leak \dot{Q}_{hl} to the BBR and the direct power P_{gen} from the excitations produced by the heater fork:

$$\dot{Q}_{hl}(\Omega) + P_{\text{gen}} = \frac{4\pi k_B P_F^2}{h^3} T e^{-\frac{\Delta}{k_B T}} (\Delta + k_B T) A_h(\Omega). \quad (4)$$

Here $A_h(\Omega)$ is the effective area of the orifice, which is reduced when part of the excitations is scattered back to the BBR.

The nuclear refrigerant is demagnetized to very low temperatures, and by further demagnetization its temperature is adjusted to remain constant. In the ballistic regime, the heat flux to the sintered heat exchanger flowing through the large 3.6-mm-diameter opening of the quartz tube or through the boundary separating the heat exchanger from the ^3He -B bath is in both cases generally assumed to be proportional to the interfacial open area A and to depend exponentially on temperature.²¹ With this assumption, the temperature below the orifice can be estimated to be less than $0.15T_c$ even when a heating of $P_{\text{gen}} \sim 15$ pW is supplied to the heater fork in the measurements. In fact, in a similar quartz cylinder, but with both division plates removed, the temperature is measured to be below $0.14T_c$ when no heating is applied, and its increase is found to be less than $0.01T_c$ at the level of heating of our measurements. This temperature is also found to depend only very weakly on the rotation velocity. This means that even when the heater is on in rotation, the quasiparticle density in the volume below the small orifice is at least two orders of magnitude lower than in the radiator above the orifice at $0.20T_c$. In our analysis, we can therefore safely omit any upward moving backflow of excitations through the orifice.

IV. REFLECTION MEASUREMENTS

In the measurement, the heater fork is driven to create the desired excitation beam corresponding to the power P_{gen} leaving the radiator. By controlling the rotation velocity, and thus the vortex density, we can control the fraction of Andreev reflected excitations. As illustrated in Fig. 2, the flow field created by the vortices reflects part of the beam back to the radiator by Andreev scattering. As a consequence, the

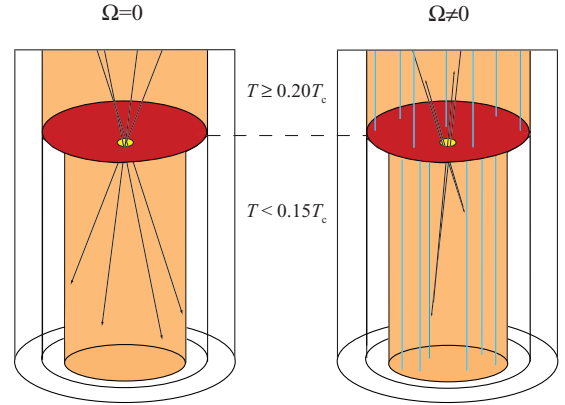


FIG. 2. (Color online) Sketch of the experiment. In the system at rest ($\Omega = 0$), all the excitations which do not migrate back to the blackbody radiator due to diffuse scattering from the walls are thermalized in the heat exchanger at the bottom. In rotation ($\Omega \neq 0$), part of the beam is Andreev reflected from the cluster of vortices below the orifice.

temperature increase above the orifice is larger than with the same applied heating in the absence of vortices. The fraction ν of heat reflected back into the radiator, which we call the reflection coefficient, can be obtained from Eq. (4) as

$$\nu(\Omega) = 1 - \frac{A_h(\Omega)}{A_h(0)}. \quad (5)$$

The radiator itself is filled with a vortex cluster, which however, does not change the excitation trajectories sufficiently to create significant thermal gradients. The main thermal resistance is across the orifice, and Eq. (5) is valid as long as there is thermal equilibrium inside the radiator. In fact, we can maintain a vortex-free state in the volume above the upper division plate in Fig. 1 up to velocities of 1.5 rad/s. We observe no changes in the temperature of the radiator volume depending on whether the upper sample volume is in the vortex-free state or in the equilibrium vortex state.

At each rotation velocity, we apply different power inputs to the radiator and measure the corresponding equilibrium temperature with the thermometer fork. By plotting all the temperature-dependent parts in Eq. (4) as a function of power P_{gen} we get a straight line (Fig. 3). From the inverse slope of the line we get the effective area A_h and from the intercept with the power axis, the heat leak \dot{Q}_{hl} .

The measurement with no vortices gives $A_h(0) \approx 0.020 \text{ mm}^2$. This is less than a half of the geometrical area A_g of the orifice. The main reason is the diffusive backscattering of the excitations from the walls of the 0.7-mm-thick division plate and the quartz tube below it. In any case, the absolute value of the effective area is not an important issue since we are only interested in the relative change in Eq. (5). The heat leak \dot{Q}_{hl} varies from 12 pW at $\Omega = 0$ to 18 pW at $\Omega = 1.8$ rad/s. At high rotation velocities the rotation-induced heat leak fluctuates with variations of about 1 pW. The rotation velocities used in the measurements had to be carefully selected, since mechanical resonances at certain velocities cause increased and temporally varying heating. Figure 4 shows the reflection coefficient as a function of the rotation velocity. In the measured rotation velocity range, the dependence of ν on the

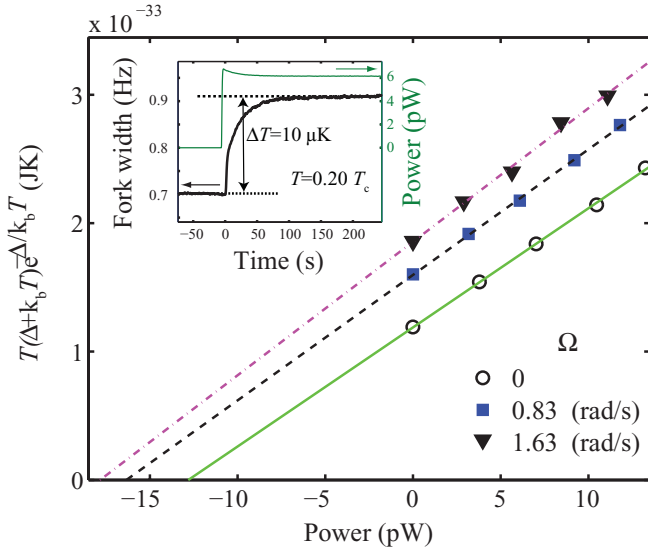


FIG. 3. (Color online) Temperature-dependent part of the power leaving the blackbody radiator as a function of heating power at three different rotation velocities. The temperature is obtained from the linewidth of the detector fork. The data points are averages from data measured for about 10 min at each power. The intercept of the linear fit with the power axis gives the residual heat leak to the sample, while the effective area is given by the inverse of the slope. The slope, the heat leak, and the scatter in the data all increase with increasing angular velocity. The inset shows an example of the detector response to a heating pulse starting at time $t = 0$.

vortex density is approximately linear. We believe that the main source of scatter in the experimental data comes from the variation of the power calibration of the heater fork.

In the measurements, the rotation velocity fluctuates on the level of $\Delta\Omega \leq 0.01$ rad/s. Therefore, it is possible that we create helical perturbations on vortex lines, which can

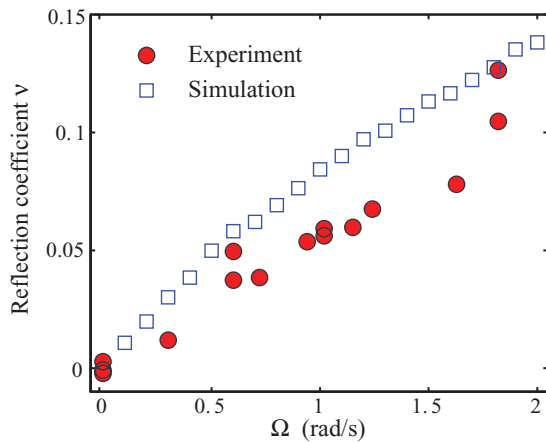


FIG. 4. (Color online) The fraction ν of the heat Andreev reflected back into the blackbody radiator, as obtained from our steady-state measurements. The temperature inside the radiator is $0.20T_c$. The simulation points are obtained by integrating Eq. (3) numerically and solving Eqs. (4) and (5) for ν . The statistical error in the absolute value of ν for the experimental data varies between 5×10^{-4} and 2.4×10^{-3} and is smaller than the size of the points. The systematic error sources are discussed in the text.

end up increasing the total vortex length and decreasing the polarization in our vortex cluster. By modulating the rotation velocity at different frequencies and amplitudes, we can study whether the presence of these perturbations, which are called Kelvin waves, affects the reflection coefficient. We find that even an order of magnitude larger modulation amplitude compared to the highest noise peaks in the rotation velocity barely affects the fraction of transmitted heat flux. Thus, we believe it is safe to omit the effect of Kelvin waves in our analysis. Our preliminary measurements at very large modulation amplitudes, however, show a decreasing fraction of transmitted heat, as expected if Kelvin waves are generated. In the future, we are hoping to utilize these techniques to study Kelvin waves in more detail.

To test whether our blackbody radiator works as expected, we can analyze how the system reaches thermal equilibrium when the heater is suddenly switched on. The expected time constant for the thermal relaxation is $\tau = RC$, where the thermal resistance across the orifice $R = (d\dot{Q}/dT)^{-1} \propto A_h^{-1}$, and the heat capacity C is given approximately by²²

$$C = k_B \sqrt{2\pi} N_F \left(\frac{\Delta}{k_B T} \right)^{\frac{3}{2}} e^{-\frac{\Delta}{k_B T}} \left(\Delta + \frac{21}{16} k_B T \right) V. \quad (6)$$

Here $V \approx 3.4 \text{ cm}^3$ is the volume of the BBR, and N_F the density of states at the Fermi level. The measured time constant is about 25 s (see inset in Fig. 3), which is in a reasonable agreement with the expected time constant (≈ 32 s) obtained using the effective area from the calibration described above. This analysis also proves that practically all the heat capacity of the system is in the bulk superfluid ^3He .

Possible error sources are the small statistical error in the determination of the slope (Fig. 3) and the uncertainties in the power calibration, the temperature calibration, and the value of the gap.²³ The reflection coefficient ν has a weak logarithmic dependence on the parameter a and depends on Δ only through the temperature calibration [Eq. (2)]. The power calibration, if time independent, has no effect on ν . We estimate the overall systematic uncertainty of the measurements shown in Fig. 4 to be of the order of the scatter in the data.

V. SIMULATION CALCULATIONS

In our numerical simulations, we calculate the transmission function T for our geometry at different rotation velocities and solve the integral in Eq. (3) numerically using Monte Carlo integration with importance sampling. For solving T , we trace whether the excitations (quasiparticles or quasiholes) leaving the BBR with properly distributed energies, directions, and positions above the orifice are reflected back or not. The simulations were done with 10^6 excitations for each rotation velocity in Fig. 4, while $A_h(0)$ was calculated using 10^7 excitations. Setting the right hand side of Eq. (4) to equal that of Eq. (3) for $\Omega = 0$ (no vortices) and $\Omega \neq 0$ (with vortices), we obtain $A_h(0)$ and $A_h(\Omega)$, which allows us to solve the reflection coefficient from Eq. (5). The simulations use the exact geometry of our experimental setup including the thickness and the shape of the radiator orifice. Instead of solving for the full equations of motions for excitations, which would require too much computing power, only the vortices for

which the impact parameter of the excitation is small enough to allow Andreev reflection are considered. We do not assume perfect retroreflection, but take into account the small Andreev reflection angle¹² $\Delta\varphi = \hbar p_F^{-1} \sqrt{\pi/(3\xi b)}$. Figure 4 shows the reflection coefficient as a function of the rotation velocity from the numerical simulations. The result is in a good agreement with the measurements.

In the simulations, diffuse scattering from the container walls is assumed based on the results in Ref. 24. In reality, part of the excitations experience Andreev reflection at the container surfaces.²⁵ Including this effect would lead to a decrease of the reflection coefficient in the numerical simulations, as confirmed by our calculations with an unrealistic steplike order-parameter variation, and improve the agreement of ν between the simulations and the measurements. The full accounting for the detailed reflection processes at diffusely scattering surfaces, including a slight particle-hole anisotropy,²⁶ would complicate the transport calculation, and we neglect these effects, arguing as follows. Our simulations with fully diffusive scattering yield a ratio $A_h(0)/A_g$ which agrees well with the known geometrical area A_g and the measured effective area $A_h(0)$. This is neither the case for the model with a steplike order parameter variation at surfaces nor for specular scattering, since to produce the measured $A_h(0)$ the former would require A_g to be roughly two times larger and the latter less than a half of the known geometrical area. Moreover, quasiclassical calculations, which model the order-parameter suppression profile in a more realistic manner,^{26,27} show that the real Andreev reflection probability at a diffusely scattering surface is only a small fraction of that in the step model. Finally, even though the details of the wall scattering processes do have an effect on $A(\Omega)$, they do not affect the reflection coefficient ν significantly compared to other uncertainties in our model.

Recent numerical studies^{28,29} indicate that especially for dense vortex structures, the total reflecting “Andreev shadow”

is not necessarily the sum of shadows of single vortices. Our clusters are relatively sparse, and moreover, after the first diffuse scattering from the walls, the probability for the excitation to migrate back to the radiator is not sensitive to small changes in its trajectory. Thus, we believe that our somewhat simplified model reproduces the real experimental situation with good accuracy. The simulations were tested at different hole radii and positions of the hole on the division plate. We find that the largest effect on the final result comes from the uncertainty of the radius: increasing or decreasing it by 50% changes the reflection coefficient by approximately $\pm 10\%$.

VI. CONCLUSIONS

In conclusion, we describe the first measurement of the interaction between thermal excitations and quantized vortices in a well-defined configuration. Numerical simulations reproduce the experimental results within the margin of uncertainty in the model. Quasiparticle beam techniques are currently the most popular measuring method of vortices in $^3\text{He-B}$ below $0.2T_c$. Our work provides a rigorous quantitative basis for their use and further development for direct visualization purposes.

ACKNOWLEDGMENTS

This work is supported by the Academy of Finland (Centers of Excellence Programme 2006-2011) and the EU 7th Framework Programme (FP7/2007-2013, Grant No. 228464 Microkelvin). J.H. acknowledges financial support from the Väisälä Foundation of the Finnish Academy of Science and Letters, and D.S. from the Czech Granting Agency under the project GAČR 202/08/0276. We also thank R. Haley, N. Kopnin, Y. Sergeev, and P. Skyba for useful discussions.

*jaakko.hosio@aalto.fi

¹W. F. Vinen, *J. Low Temp. Phys.* **161**, 419 (2010).

²E. A. L. Henn, J. A. Seman, G. Roati, K. M. F. Magalhães, and V. S. Bagnato, *Phys. Rev. Lett.* **103**, 045301 (2009).

³R. J. Donnelly, *Quantized Vortices in Helium II* (Cambridge University Press, Cambridge, 1991).

⁴P. M. Walmsley, A. I. Golov, H. E. Hall, A. A. Levchenko, and W. F. Vinen, *Phys. Rev. Lett.* **99**, 265302 (2007).

⁵M. S. Paoletti, Michael E. Fisher, K. R. Sreenivasan, and D. P. Lathrop, *Phys. Rev. Lett.* **101**, 154501 (2008).

⁶L. Skrbek and W. F. Vinen, in *Progress in Low Temperature Physics*, edited by M. Tsubota and W. P. Halperin (Elsevier B. V., Amsterdam, 2009), Vol. XVI, p. 195.

⁷V. B. Eltsov, R. de Graaf, R. Hänninen, M. Krusius, R. E. Solntsev, V. S. L'vov, A. I. Golov, and P. M. Walmsley, in *Progress in Low Temperature Physics*, edited by M. Tsubota and W. P. Halperin (Elsevier B. V., Amsterdam, 2009), Vol. XVI, p. 45.

⁸V. M. H. Ruutu, U. Parts, J. H. Koivuniemi, N. B. Kopnin, and M. Krusius, *J. Low Temp. Phys.* **107**, 93 (1997).

⁹R. Hänninen, R. Blaauwgeers, V. B. Eltsov, A. P. Finne, M. Krusius, E. V. Thuneberg, and G. E. Volovik, *Phys. Rev. Lett.* **90**, 225301 (2003).

¹⁰S. N. Fisher and G. R. Pickett, in *Progress in Low Temperature Physics*, edited by M. Tsubota and W. P. Halperin (Elsevier B. V., Amsterdam, 2009), Vol. XVI, p. 147.

¹¹A. F. Andreev, *Zh. Eksp. Teor. Fiz.* **46**, 1823 (1964) [*Sov. Phys. JETP* **19**, 1228 (1964)].

¹²C. F. Barenghi, Y. A. Sergeev, and N. Suramlshvili, *Phys. Rev. B* **77**, 104512 (2008).

¹³M. P. Enrico, S. N. Fisher, A. M. Guénault, G. R. Pickett, and K. Torizuka, *Phys. Rev. Lett.* **70**, 1846 (1993).

¹⁴D. I. Bradley, S. N. Fisher, A. M. Guénault, M. R. Lowe, G. R. Pickett, A. Rahm, and R. C. V. Whitehead, *Phys. Rev. Lett.* **93**, 235302 (2004).

¹⁵A. M. Guénault and G. R. Pickett, *Physica (Amsterdam)* **126B**, 260 (1984).

¹⁶R. Blaauwgeers *et al.*, *J. Low Temp. Phys.* **146**, 537 (2007).

- ¹⁷D. I. Bradley, P. Crookston, S. N. Fisher, A. Ganshin, A. M. Guénault, R. P. Haley, M. J. Jackson, G. R. Pickett, R. Schanen, and V. Tsepelin, *J. Low Temp. Phys.* **157**, 476 (2009).
- ¹⁸P. Skyba, *J. Low Temp. Phys.* **160**, 219 (2010).
- ¹⁹D. I. Bradley, M. Človečko, E. Gažo, and P. Skyba, *J. Low Temp. Phys.* **151**, 147 (2008).
- ²⁰M. Krusius, J. S. Korhonen, Y. Kondo, and E. B. Sonin, *Phys. Rev. B* **47**, 15113 (1993).
- ²¹C. A. M. Castelijns, K. F. Coates, A. M. Guénault, S. G. Mussett, and G. R. Pickett, *Phys. Rev. Lett.* **55**, 2021 (1985).
- ²²C. Bäuerle, Y. M. Bunkov, S. N. Fisher, and H. Godfrin, *Phys. Rev. B* **57**, 14381 (1998).
- ²³I. A. Todoschenko, H. Alles, A. Babkin, A. Ya. Parshin, and V. Tsepelin, *J. Low Temp. Phys.* **126**, 1449 (2002); we use the gap $\Delta(0) = 1.968T_c$ at 29 bar pressure.
- ²⁴M. P. Enrico and R. J. Watts-Tobin, *J. Low Temp. Phys.* **102**, 103 (1996).
- ²⁵G. Kieselmann and D. Rainer, *Z. Phys. B* **52**, 267 (1983).
- ²⁶W. Zhang, J. Kurkijärvi, D. Rainer, and E. V. Thuneberg, *Phys. Rev. B* **37**, 3336 (1988).
- ²⁷W. Zhang and J. Kurkijärvi, *J. Low Temp. Phys.* **73**, 483 (1988).
- ²⁸C. F. Barenghi, Y. A. Sergeev, N. Suramlishvili, and P. J. van Dijk, *Phys. Rev. B* **79**, 024508 (2009).
- ²⁹C. F. Barenghi, Y. A. Sergeev, N. Suramlishvili, and P. J. van Dijk, *Europhys. Lett.* **90**, 56003 (2010).